48th AIAA/ASME/SAE/ASEE Joint Propulsion Conference & Exhibit
30 July - 01 August 2012, Atlanta, Georgia

AIAA 2012-3929

Numerical and experimental efforts to explain delayed gas breakdown in θ-pinch devices with bias magnetic field

Warner C. Meeks* and Joshua L. Rovey†

Missouri University of Science and Technology, Rolla, Missouri, 65409, USA

A single particle model and particle-in-cell simulations have been used to elucidate the breakdown physics in a ringing theta-pinch with a bias magnetic field. Previous experimental results show that gas breakdown occurs when the bias magnetic field is nullified by the theta-pinch magnetic field. The analyses presented here agree with the experimental results and show that electron kinetic energy does not exceed the ionization threshold of deuterium until the net magnetic field is approximately zero. Despite the presence of a strong electric field, the gyromotion of electrons within the bias magnetic field prevents them from gaining energy necessary to ionize the gas. Parametric analysis of the peak electron energy as a function of the bias and pre-ionization magnetic fields reveals that: (1) when the bias magnetic field is $\approx$ 97% of the pre-ionization magnetic field, peak electron energies are highly erratic resulting in poor overall ionization, and (2) full ionization with repeatable behavior requires a pre-ionization to bias magnetic field ratio of approximately 2 to 1 or higher. Efforts to better characterize this phenomena experimentally are ongoing. However some preliminary findings using a dual-probe cancellation technique are presented.

I. Introduction

THE theta-pinch concept is one of the most widely used inductive plasma source designs ever developed. It has established a workhorse reputation within many research circles, including thin films and material surface processing,[1–3] fusion,,[4–6] high-power space propulsion,[7,8] and academia,[9,10] filling the role of not only a simply constructed plasma source but also that of a key component. In superconductive thin films, theta-pinch ionization has been used as an electrodeless alternative ion injection source. Recently, University of Illinois at Urbana-Champaign has developed the Divertor Erosion and Vapor Shielding eXperiment (DEVeX), a theta-pinch plasma source to study vapor shielding of lithium surfaces exposed to plasmas. Several theta-pinch schemes have been used worldwide since the 1970s to form field reversed configuration (FRC) plasmoids for use in fusion proof-of-concept studies and experiments.[11,12] In recent years, interest in future high power space electric propulsion (EP) concepts involving the formation and acceleration of heavy gas (i.e., Ar, Xe, etc.) FRCs via theta-pinch coils has grown in both the public and private sectors.[13,14] Despite a long history of research and utilization, initial onset ionization mechanisms in theta-pinch plasmas often go overlooked or under-appreciated due to either a primary interest in the quasi-steady state conditions (in films and materials surface processing and academia), insufficient high-speed ($< 10^{-7} - 10^{-8}$ s) diagnostics (in fusion and propulsion studies), or a larger interest in the high energy, high density final state of the plasma (in fusion and materials processing).

Theta-pinch devices utilize relatively simple coil geometry to induce electromagnetic fields and create plasma. A typical theta-pinch coil consists of a single-turn that wraps cylindrically around a gas while current, $\boldsymbol{I}$, flows in an azimuthal direction. Ignoring end effects, this current induces a uniform axial magnetic field, $\boldsymbol{B}$. Often an initial bias magnetic field is applied, opposite in axial orientation to latter stages, by a quasi-steady current (steady with respect to subsequent discharges, $f_{bias} \approx 1$ to 10s of kHz), which has

*Gradute Research Student, Mechanical and Aerospace Engineering, wcm994@mst.edu, AIAA Student Member.
†Assistant Professor, Mechanical and Aerospace Engineering, roveyj@mst.edu, AIAA Senior Member.

been shown over several studies to improve formation by way of either plasma preheating or increasing the trapped magnetic flux.[15–18] When the axial magnetic field is changing in time (i.e., dI/dt $\neq$ 0), it induces an electric field, $\boldsymbol{E}$, described by Faradays law (stated by Eq. (1) for reference) that opposes the changing current. This process is illustrated in Figure 1(a), which shows a cut-away of typical theta-pinch operation during an initial current rise.

$$\text{Faraday's Law: } \oint \vec{E} \cdot \vec{dl} = \frac{-d}{dt} \int \vec{B} \cdot \vec{dA}. \tag{1}$$

The current rise (and subsequent ringing time-domain profile) is essentially the result of a typically under-damped LRC circuit where the coil represents the principal inductance (L) and is driven by a high voltage (10s to 100s of kV) capacitor bank (C). Some theta-pinch test experiments utilize multiple discharge stages with the first post-bias discharge commonly referred to as pre-ionization. Pre-ionization (PI) stages are typically characterized by lower energies at higher frequencies relative to the final main discharge (i.e., $f_{PI} > f_{main} \gg f_{bias}$). Typical theta-pinch ringing discharge frequencies range from 100s of kHz to 10s of MHz depending on the stage. While implementation of bias fields have become commonplace in theta-pinch devices for fusion and EP studies, they remain a point of contention in terms of how best to implement them and ultimately whether or not they are as useful (i.e., necessary) as reported in literature.

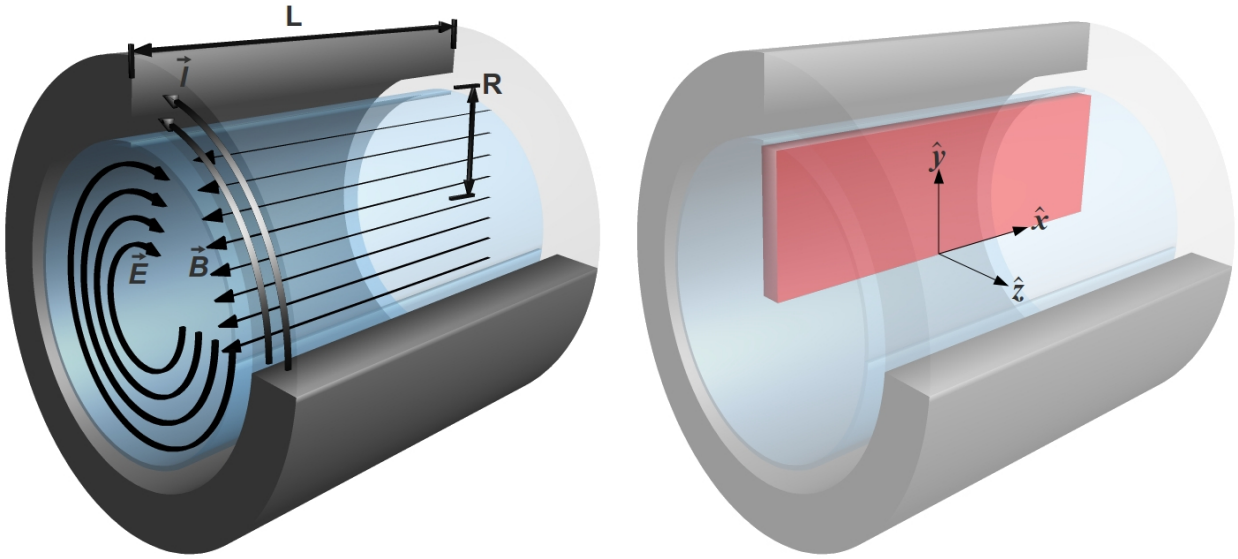

(a) (b)

Figure 1: (a) Ideal theta-pinch field topology for an increasing current, I. (b) Analogous Cartesian geometry simulated (red) using planar approximation.

Early work on the Scylla I theta-pinch device during the 1960s at Los Alamos National Laboratory (LANL) by Little et al. demonstrated that both strong preionization and a bias field B_0 antiparallel to the main compression field B_z are necessary to produce neutrons during the first half-cycle of the discharge.[15] The Scylla I device produced bias and main discharge fields of 400 and 5500 mT, respectively. Also, in 1966, experiments on the Megajoule Theta-Pinch at the Culham Laboratory in the U.K. by Green and Newton attempted to provide explanation for losses in trapped bias flux when the bias field is sufficiently high ($B_0 \approx 300mT$).[19] Authors of that work proposed that a portion of the initial bias flux is lost almost immediately when applied magnetic field passes through zero (onset by field reversal). Plasma would rebound and briefly come into contact with the walls, neutralizing electrons and releasing the portion of magnetic field retained by these electrons. Experimental results reported during the 1980s on the Field Reversed eXperiements (FRX-A[16] and FRX-B[20]) also at LANL, highlighted the significance of the bias magnetic field nullification (referred therein as net magnetic field zero-crossing) by the ringing theta-pinch field profile in providing high levels of ionization.[20] Bias and PI field magnitudes were reported to be 70 and 110 mT, respectively, for FRX-A and 230 mT for both in FRX-B. However, the FRX-A,B reports appear to have provided only observations without explanation for why this zero-crossing is critical.

Since around the turn of the 21st century collaborative efforts between the Air Force Research Laboratory (AFRL) and LANL have focused on the use of FRCs to demonstrate feasible, very high temperature, high density mass delivery systems for fusion, and high energy density plasma research.[5,6,21,22] First from around 2000 to 2007 with the Field Reversed eXperimentw/Liner (FRX-L) at LANL and then in 2007 constructing the Field Reversed Configuration Heating eXperiment (FRCHX) at AFRL-Kirtland.[21,22] These proof-of-concept studies seek to conduct FRC capture and compression with the goals of demonstrating magnetized target fusion (MTF) and studying the high energy density plasma state. As with earlier results, ionization is reported to form when the bias field has been approximately nullified (see Figure 2) by the first ring of the theta-pinch PI field, when dB/dt approaches zero (i.e., when electric field is at its weakest).[21] While the earlier recommendations of Armstrong et al. suggest to incorporate this zero-crossing, for the FRCHX experiments, this leads to an initial plasma formation with little to no trapped magnetic flux in turn, reducing FRC lifetime. In addition to this, the FRCHX results seem to contradict what an electrostatic approach for ionization would predict, which is that the greatest levels of ionization would occur when the electric field is first peaked (i.e., when the theta-pinch PI is initially triggered). At present, there is no explanation for what is occurring during this early time and why there is a delay in plasma formation to the net magnetic field zero-crossing.

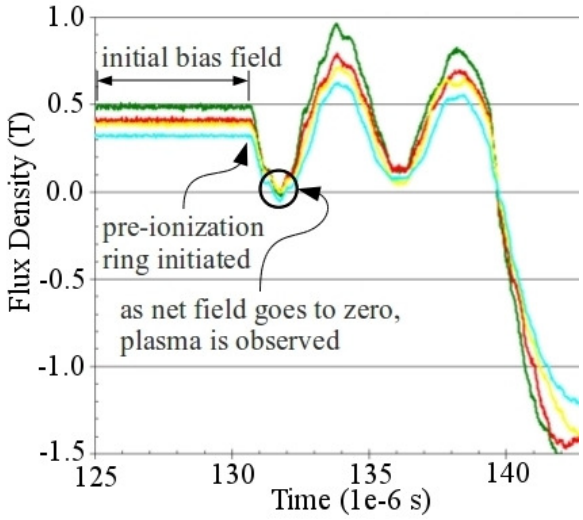

Figure 2: Reported magnetic field results (integrated B-dot probe data) from FRCHX (Ref. 21).

Research published previously by the authors provides explanation for some of these on-going observations.[23] To gain insight into the fundamental kinetic effects that bias fields introduce in a theta-pinch device, interpreted magnetic and electric fields and geometry from FRCHX were used as test case data for both an analytical single electron and particle-in-cell (PIC) study. These insights have elucidated the electron kinetic phenomena during onset of the breakdown processes when a bias magnetic field is present. In addition to the afore mentioned insights and explanations, some of the follow-on experimental work to provide additional verification is presented here. Impacts of these results on theta-pinch operation in general are then assessed.

II. Approach

II.A. Assumptions

Three principle assumptions were used in the simulations and analyses presented here. These are as follows: (1) fields consist of only a uniform, axial magnetic field and an azimuthal electric field, (2) the problem is static (i.e., fields are constant) over short time intervals of approximately 10 ns, and (3) fields follow the planar simplification: $\mathbf{B} = B_x(t)\hat{x}$ and $\mathbf{E} = E_z(y,t)\hat{z}$. Assumption (1) simply implies that end effects such as magnetic mirroring, diverging electric fields, etc. are ignored. Assumption (2) is justified in a window of 10 ns for this study by reported results of FRCHX (Figure 2). In these results, during the first ¼-cycle

of the pre-ionization ring (e.g., $0 \leq t \leq t_{1/4}$), the magnetic field is seen to decrease sinusoidally from an initial value of 500 mT to approximately zero in 1 μs. This corresponds well with a reported pre-ionization circuit frequency of 230 kHz ($t_{1/4} \approx 1.09\mu$s). From here, it is assumed that 10 ns $\ll t_{1/4}$ and subsequently $\mathbf{B}(t) \approx B(t + 10$ ns). Assumption (3) of planar fields ($\mathbf{B} = B_x, \mathbf{E} = E_z$) stems from a focus here on an r-z plane, which is then converted to an analogous Cartesian geometry as shown in Figure 1(b). By extension, this assumption also implies the common use of azimuthal symmetry and ignores bulk motion azimuthally that could be due to (for instance) diamagnetic drifts as plasma density becomes non-uniform.

II.B. Approximation of Fields

A sinusoidally time-varying magnetic field profile modeled after reported FRCHX data (i.e., amplitude, frequency, etc.) is applied to Faradays law to provide approximation of the induced electric field. Nomenclature for Faradays Law in a theta-pinch device follows using common ideal solenoid analyses. For uniform, orthogonal fields Eq. (1) is simplified to

$$E = \left(\frac{-dB}{dt}\right)\frac{r}{2} \tag{2}$$

for approximation of the time-dependent electric field magnitude. The magnetic field is modeled by an inverted sine function with a positive offset matching the initial bias of 500 mT. Device frequency, f, is approximated to be 250 kHz (frequency reported to be approximately 230 kHz in the actual FRCHX test experiment[21]) for a ¼-cycle time of 1 μs and the appropriate equation for the time-varying magnetic field of

$$B(t) = -0.5\sin(2\pi f t) + 0.5 \text{ (T)}. \tag{3}$$

Plots of approximated field profiles can be seen overlaid with FRCHX results in Figure 3 for an ambiguous radial value. From here, cylindrical coordinates are approximated to Cartesian coordinates by the nomenclature seen in Figure 1(a). For clarity, this transition is also stated in

$$B(t)\hat{z}_{cyl} \rightarrow B(t)\hat{x}_{cart} \tag{4}$$

$$E(r,t)\hat{\theta}_{cyl} \rightarrow E(y,t)\hat{z}_{cart}. \tag{5}$$

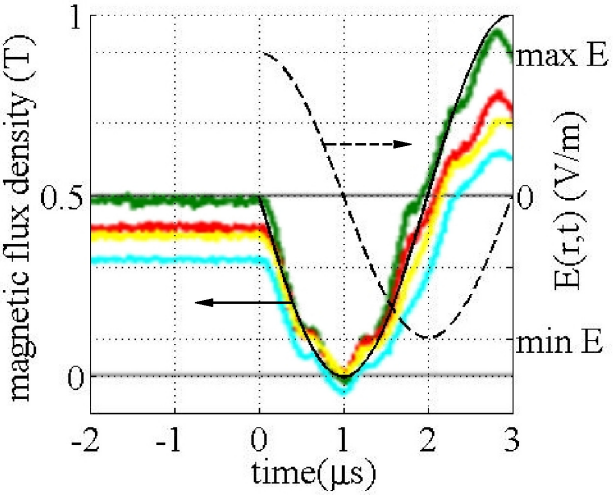

Figure 3: Reconstructed field profiles with original reported FRCHX results.

II.C. Applied Methods

The single particle model uses the straightforward 2-D equations of oscillatory motion in orthogonal electric and magnetic fields. Using the nomenclature presented in Figure 1(b) for a magnetic field purely in the axial

($\hat{x}$) direction and an electric field purely in the azimuthal ($\hat{z}$) direction these equations for electron motion reduce to

$$\frac{d\vec{v}_y}{dt} = \frac{e}{m_e}(0 + v_z \cdot B_x)\hat{y}, \text{ and} \tag{6}$$

$$\frac{d\vec{v}_z}{dt} = \frac{e}{m_e}(E_z - v_y \cdot B_x)\hat{z}. \tag{7}$$

The freely available UniX based Object-Oriented Particle-In-Cell code XOOPIC,[24,25] developed originally at U.C. Berkeley, is utilized to model ionization at early times in a deuterium gas for a pseudo theta-pinch geometry. This code is a 2-D, relativistic, Monte Carlo collisional code that can be modeled electrostatically or, if curling electric fields lie only on a 2-D solution plane, can solve electrodynamic problems as well. Before ionization studies were undertaken, efforts were made to ensure reasonable accuracy of the code and proper implementation of the particle physics. The geometry parameters used were a characteristic length of half the total length of FRCHX, or 18.2 cm and a constant radius of 6.5 cm. These parameters were chosen to capture the mid-section of a theta-pinch coil like FRCHX and provides a simulation length to diameter ratio, $L/D = 1.4$.

Additional information on the implementation of these methods as well as verification of the XOOPIC code against theoretical calculations of electron-cyclotron frequency, gyro-radius, and $\mathbf{E}\times\mathbf{B}$ drift velocity can be found in the authors previous work.[23]

III. Results and Analysis

III.A. Single electron energy results

Figure 4 shows time-resolved kinetic electron energy data for the applied fields shown in Figure 3. Used in all of these studies, the initially cold electrons start with a kinetic energy of zero. However, despite large initial electric fields, kinetic energy remains low and varies minimally until approximately 0.9 μs. For this reason, Figure 4 focuses on a time frame of 0.85 to 1.1 μs only. By 0.9 μs, the applied magnetic field, as seen earlier in Figure 3, has been reduced by nearly 99% from 500 to 6.2 mT, compared with a reduction of 84% for the electric field (12.76 to 2.0 kV/m). Just 37 ns after the magnetic field zero-crossing (i.e., $t_{1/4}$+0.037 μs), the oscillatory electron energy crosses the gaseous D_2 ionization threshold, $I_{g,D2}$, of 15.47 eV. Following this, at approximately 1.05 μs, energy peaks at 32.2 V (not shown) corresponding to a velocity magnitude of 3.35×10^6 m/s. This time at which the electron energy peaks corresponds to a field magnitude of 1.5 mT which, when combined with the velocity magnitude, yields a Larmor radius of 1.2 cm.

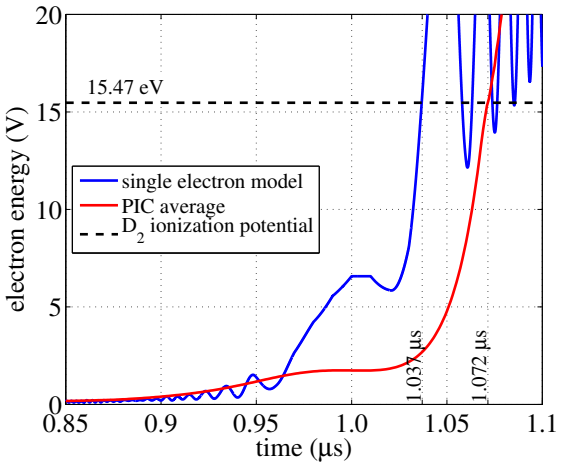

Figure 4: Kinetic energy for both the single electron energy study and iterative PIC study. Initially cold, v=0 m/s electrons.

This simple analysis of the single electron kinetics for orthogonal time-varying fields shows that, from rest and for the field profiles approximated from FRCHX data, the electron only achieves deuterium level

ionization energies just after the magnetic field goes to zero. This agrees qualitatively with reported ionization results of FRCHX. However, it is worth restating that in this simple analysis a single radial location was used thus ignoring the transition to higher electric field magnitudes as electrons drift radially outward by **E**×**B** GC drifts. This is, of course, a common physical result of real theta-pinch devices. However, the electric field from R/2 to R is easily seen to simply double in magnitude, ignoring space charge effects. Also, no boundary conditions were set keeping electron energy from being lost to the walls nor is a background gas present to allow energy losses via collision processes as electrons approach the deuterium excitation energy ($\approx$ 14.9 eV).

III.B. Iterative PIC results

Figure 4 also shows time-resolved electron kinetic energy results from the iterative PIC approach as outlined above against the earlier single electron results. Both elastic and ionization collisions are modeled and can be seen to remove some energy from the super-thermal (or near-beam) energy distribution for times at and following $t_{1/4}$. Loss of electron energy to excitation and ionization collisions is suspected by the authors to also be the cause of a difference in time that the ionization threshold is reached between the single particle and PIC study ($t_{1/4}$+0.037 μs vs $t_{1/4}$+0.072 μs, respectively). It can be seen from Figure 4 that while average energy lags that of the single particle case, trends of the PIC study still correspond with the delayed ionization reported by FRCHX. It should be noted that a deuterium collisional cross-section table was not natively available in XOOPIC and thus the table for gaseous diatomic hydrogen ($I_{g,H2}$ = 13.6 eV) was used as a substitute in these particle-in-cell studies.

III.C. Electron energy performance in B_{bias}-B_{PI} space

To analyze additional experimental conditions, a parametric study using the above single particle approach has been conducted by revisiting Eq. (3) and generalizing for a time-varying net magnetic field

$$B_{net}(t) = -B_{PI}\sin(2\pi f t) + B_{bias}\ (\mathrm{T}). \tag{8}$$

Here, B_{PI} denotes the amplitude of the pre-ionization stage. However, this component can represent a main discharge as well if PI is not present. To fill out a 3-D performance space, B_{bias} and B_{PI} magnitudes are varied individually and peak electron energy is found and plotted for all combinations therein. In all combinations, electric field has been evaluated in the same manner as above, which is that the electric field at half radius (3.25 cm) is used. In the interest of computation time, three ranges for B_{bias} and B_{PI} are assigned individually, and data are then spliced together post-process. This is evidenced by the three squares of color data in Figure 5 overlapping at the corners corresponding to the three ranges tested. The area of white-space above-left and below-right in Figure 5 was not simulated, but trends in these areas can be extrapolated from the neighboring regions investigated. Magnetic field ranges tested were: B_{bias}, B_{PI} = 0-350, 300-700, and 650-1050 mT. Ranges were picked to overlap by 50 mT to verify smooth transition of values from one data-set to the next.

Figure 5 shows the results of this additional analysis by plotting the maximum electron energy (normalized to 1600 eV) seen in each combination of B_{bias} and B_{PI}. Values in the figure represent the first electron peak in the discharge cycle (i.e., only the first ½-cycle has been modeled). With some explanation, it can be seen from Figure 5 that three regions of electron energy activity arise. First is a region of low peak electron energy for the case of $B_{bias} \geq B_{PI}$ seen starting in the lower right of each range of field values (shown in dark blue in the lower-right of each data set). In this region, the net magnetic field is either not nullified and a zero-crossing never occurs or is just made to reach zero as electric field does so at the same time (i.e., B_{net} = 0 as $dB_{net}/dt = 0$). Subsequently, electron energy remains low (or just approaching ionization levels). It is in this region that FRX-B and FRCHX are operated.

Transitioning then to a second region in Figure 5, where B_{bias} consistently falls just below B_{PI} (B_{bias} $\approx$ 97% of B_{PI}) yields a semi-random distribution of high energy values cutting diagonally through the figure from bottom left to upper right. It is noted here that verification that this region is not the result of numerical error or non-convergence was addressed. To this effect, time-resolved electron energy profiles for these B_{bias}, B_{PI} values appeared smooth over time and thus seemingly random peak energies in this region appear to be only the result of constructive (or destructive) timing between electron gyromotion and zero-crossing(s). Theta-pinch test experiments operated in this region capitalize on the consequence of the sinusoidal nature of the field profiles (see Figure 3), wherein the magnetic field is reduced significantly earlier

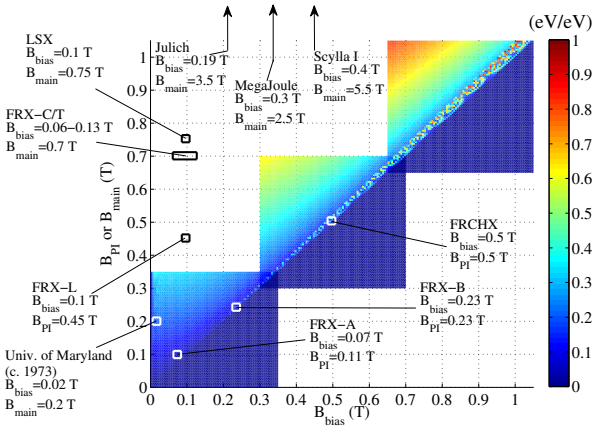

Figure 5: Peak electron energy (normalized to maximum of 1600 eV) for varying bias and pre-ionization magnetic fields. Performance data points from various actual theta-pinch test experiments are overlaid for reference.

as time approaches $t_{1/4}$ while electric field remains high for these same times. For instance where $B_{bias} \approx 97\%$ of B_{PI}, $E(t_{1/8}) = 71\%$ of E_{max} while in contrast $B(t_{1/8}) = 29\%$ of B_{max}. This provides a short time frame in which electrons are able to accelerate under a large electric field while relatively unrestricted by magnetic field. The stark contrast between these first two regions reveals that a brief zero-crossing gives electrons a small amount of extra acceleration time before electric field passes through zero. Unfortunately, timing of both net field zero-crossing and gyromotion become critical in this second region and peak electron energies prove to be quite erratic with respect to B_{bias}-B_{PI} space. It should be noted however that for an actual multi-particle environment this peppering of high energy cases in the second region would be greatly affected (most likely softened) by collisional processes and peak energies in this region will most likely be inversely proportional to backfill gas pressure.

Finally, a third region follows for further reducing B_{bias} ($B_{bias} < 0.97B_{PI}$, or equivalently an increased B_{PI}), and peak energy trends as a smooth gradient of increasing peak electron energy for increased B_{PI}/B_{bias}. Here, the net magnetic field passes through zero at earlier times while the electric field profile remains unchanged when considering a line of decreasing B_{bias} for constant B_{PI} (because electric field is only a function of B_{PI} and discharge frequency). This appears to be the ideal region in which to operate a theta-pinch based on its desirably well-behaved and predictable peak energy trend. However, as the electric field is increased (i.e., larger dB/dt, leading to greater particle acceleration) for an earlier zero-crossing net magnetic field, charged particle losses to the walls of the device would become the predominant concern.

Figure 5 also shows design point call-outs corresponding to field magnitudes reported from previous theta-pinch experiments. It is noted here that a PI discharge is not present in all theta-pinch test experiments (such as early theta-pinch experiments of the 1960s) and in these cases where PI is not present B_{PI} magnitude represents instead the main inductive discharge magnitude. Thus it is re-iterated that post-bias simply refers to whichever discharge immediately follows the applied bias field. It is also noted that this analysis assumes the post-bias inductive discharge, whether it be PI or main, is timed to occur at the peak of the bias field. If this is not the case then B_{bias} here would represent the magnitude of the bias field at the time of discharge for the post-bias field. Additionally, while the results of Figure 5 are for a constant post-bias field frequency of 250 kHz, the trends seen here have been verified to hold down to at least 125 kHz and up to at most 500 kHz with the only difference being a shift down or up in peak energies, respectively. It is concluded then that the characteristic regions described for Figure 5 are applicable over the entire frequency range of typical theta-pinch post-bias coil discharges. Analyses of Figures 3 and 5 are used to study how the electric field magnitude at the time of the net magnetic field zero-crossing, $E_{B=0}$, changes as a function of B_{bias} and B_{PI}.

Figure 6 shows this relationship for lines of constant pre-ionization magnetic field ($B_{PI} = 0.05$, 0.3, 0.55, 0.8, and 1.05 T shown), and it can be seen that the highest values of $E_{B=0}$ occur as bias field offset, B_{bias}, approaches zero (left side of the figure).

This becomes obvious when referred back to Figure 3 and the net magnetic field profile imagined to shift downward as initial bias field offset is reduced. The net magnetic field crosses zero at earlier times and

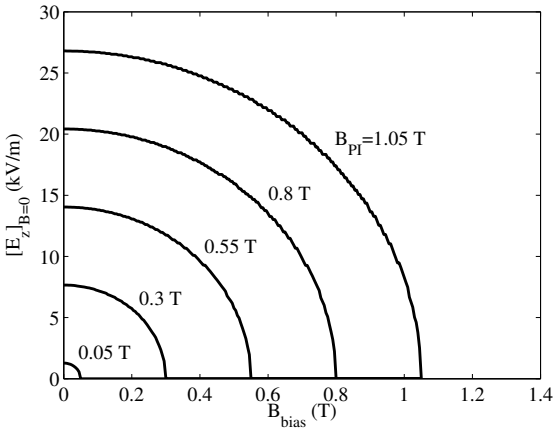

Figure 6: Electric field magnitude at the time of net magnetic field zero-crossing for select lines of constant pre-ionization magnetic field.

electric field corresponding to these earlier times is higher (because dB/dt is larger), thus yielding the results in the 3rd region of Figure 5 (described above where B_{bias} = 40% to 60% of B_{PI}) as well as the results of Figure 6. Across all cases, $E_{B=0}$ remains above approximately 90% of its maximum for B_{PI}/B_{bias} ratios of 2 to 1 or higher. The reader is reminded that the electric field (to the extent addressed in this work) is affected by B_{PI} and frequency only. Conversely as B_{bias} approaches a given B_{PI}, $E_{B=0}$ is reduced to zero. Again this is explained by reference to Figure 3. As B_{bias} approaches the same value as B_{PI} (e.g., as one approaches the conditions of FRCHX), $E_{B=0}$ converges on the value at quarter-cycle time, $t_{1/4}$. This is of course where $dB/dt=0$ and subsequently $E(y,t)=0$. Further increasing B_{bias} past B_{PI} means that net magnetic field never reaches zero and thus electrons never see the (albeit brief) period of unrestricted acceleration and electron energies remain very low. This corresponds to the first region described in Figure 5 (dark blue).

IV. Efforts in experimental verification of delayed breakdown

Work is currently underway by the authors to document the above phenomena in their own theta-pinch test article. The Missouri Plasmoid Experiment (MPX) is a single stage axis-symmetric theta-pinch device with a one turn copper coil.[26] The rolled copper sheet coil has a diameter of 18 cm and a length of 76.2 cm. This device does not presently have a bias magnetic field circuit in conjunction with its ringing theta-pinch circuit. However, recently taken internal probe data show direct indications of the delay in gas breakdown at early times until the magnetic field magnitude experiences a zero-crossing.

The high-speed probe technique used here for internal plasma diagnostics is of a similar concept to that pioneered by Lobbia and Gallimore.[27] In this technique, in addition to a single Langmuir probe, a second probe insulated from direct particle interaction but un-shielded from RF noise is placed at approximately the same location. When dealing with high-speed pulsed devices a process such as this is critical to accurate probe measurements due to the generally high levels of RF noise present. The size of the two probe collectors (exposed and insulated conductors) are identical in dimension and all lengths and types of wiring used are also identical. Once data is collected by each probe simultaneously the insulated probe signal is subtracted off from the exposed probe post-process. Thereby effectively eliminating any non-plasma artifacts from the exposed probe signal. Figure 7 shows the assembled configuration of dual Langmuir probes used by the authors. The probes used here were constructed of RG223/A double-shielded co-axial cable with the inner silver-plated solid copper conductor exposed (i.e., double-shielding removed) to a length of 8.5 millimeters. This provides a length to diameter ratio of, $L/D = 9.5$.

Figure 8 shows discharge current along with the corrected (subtracted RF noise) voltage of the exposed probe for a charge voltage of 15 kV and a peak current of 26 kA at 0.6 μs. Discharge voltage is dissipated in approximately 20 μs at a frequency of 440 kHz. While voltage potential on the exposed probe only is a clear indication of plasma interaction, it is not necessarily an accurate indication of when gas breakdown first occurs in the theta-pinch device as a whole. However, for the case shown the dual probes were located 2 cm

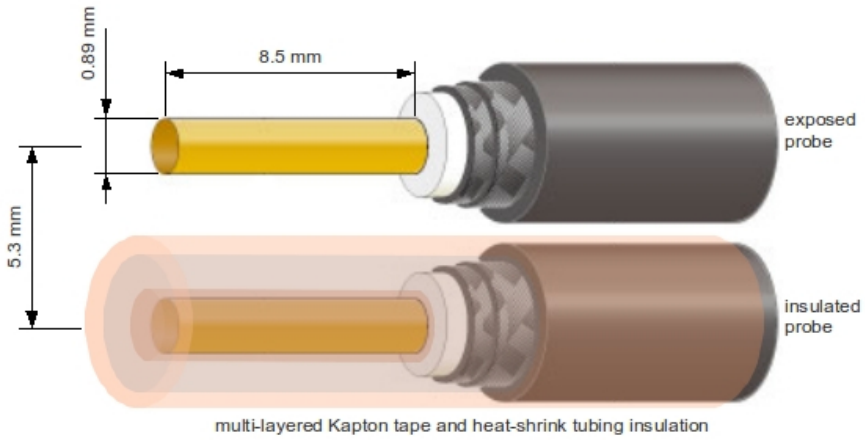

Figure 7: Dual Langmuir probe configuration used in MPX.

radially inward from the inner theta-pinch wall (i.e., $r = 0.78 \cdot R$) and at the axial mid-length of the device. Furthermore, as seen from Eq. 2, electric field increases with radius and thus at a probe location of 78% of R, electric field magnitude will be near that of the maximum seen at the inner wall. It is observed then from Figure 8 that gas breakdown does not occur until after the first ½-cycle of discharge current. Since magnetic field and current in a theta-pinch device are directly proportional, it is further inferred then that gas breakdown does not occur until the magnetic field magnitude has first passed through a zero value. It is reiterated here that this discharge does not presently utilize a bias magnetic field and thus shows a delay in gas breakdown even for the unbiased case. Delayed breakdown until after the first ½-cycle for an unbiased device has been reported before by Humphries, *et al.*[28] in which a planar pulsed inductive device is used. In that work, similarly to the results reported here, inhibited electron motion due to the magnetic field is cited as the reason for delay. Future work by the authors is focused on better characterization of what affects this delay and mapping of the plasma motion during a ring full discharge. What bearing location, pressure, and gas species have on the delay of breakdown are among the first questions intended to be addressed.

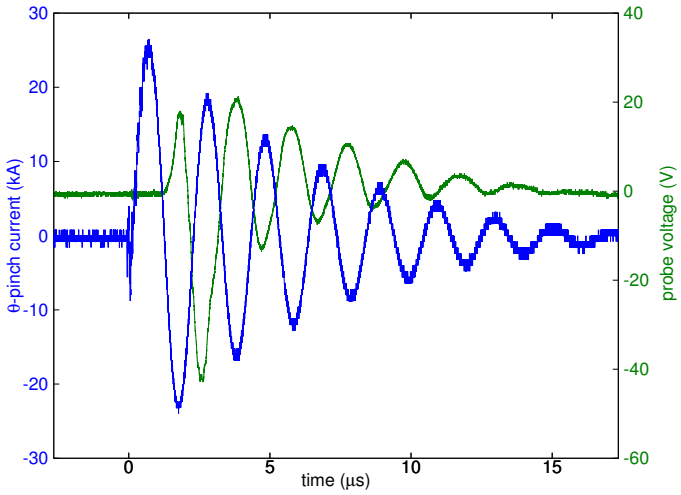

Figure 8: MPX discharge profiles for theta-pinch coil current and exposed probe voltage for a 15 kV charging voltage.

V. Conclusions

Reported results from several theta-pinch experiments arrive at the same conclusion that ionization can be dictated (i.e., inhibited) by improper choice of the bias magnetic field magnitude and the post-bias stage that follows (post-bias being either a pre-ionization or main discharge field, depending on the device). This

fact is further substantiated by single particle and particle-in-cell studies presented here. These models were first verified against each other yielding 37 and 72 ns delays (past quarter-cycle discharge time) in reaching gaseous deuterium ionization levels for single particle and particle-in-cell studies, respectively, each using FRCHX design characteristics. Subsequently, further inspection against FRCHX has shown good qualitative agreement from both models with reported results from Grabowski et al.[21]

Additional studies were then performed to better describe the relationship between electron energy and (bias and post-bias) magnetic field magnitudes. Specifically demonstrated in this work is the fact that electron energy remains minimal until the post-bias magnetic field magnitude is at least approximately 3% higher than the bias field magnitude. In general, having a larger post-bias discharge magnitude over that of the bias is shown to allow a critical net magnetic field zero-crossing, which proves imperative in triggering ionization level electron energies. In addition, it is demonstrated that a near-matched set of bias and post-bias magnetic field magnitudes does not yield well-behaved and predictable electron energies making designed performance difficult to impossible. Also, it is shown graphically that the electric field present at the time of zero-crossing of the net magnetic field is increased substantially for decreased bias field magnitude. Ultimately, results presented here show that a desired ratio of post-bias to bias magnetic field magnitudes is on the order of 2 to 1 or higher.

This effect of delayed breakdown is also seen in *unbiased* pulsed inductive devices as well further re-enforcing the concept that direct inhibition of electron motion is the primary factor. Efforts by the authors as well as past research show that at least the first ½-cycle is required for breakdown allowing magnetic field to first experience a zero-crossing.

Acknowledgments

The authors would like to gratefully acknowledge the Air Force Office of Scientific Research (Grant No. FA9550-10-1-0204) and Dr. Mitat Birkan as well as the Missouri Research Board for their support of this work. Also, special thanks to Dr. David Kirtley (MSNW) and Dr. Scott Kovaleski (University of MissouriColumbia) for sharing their insights and experiences involving pulsed inductive plasmas and modeling as well as Dr. John Verboncoeur and the members of the OOPIC Users Group.

References

[1]Surla, V., Jaworski, M. A., Gray, T. K., Ibano, K., Xu, W., Neumann, M. J., and Ruzic, D. N., "Lithium research as a plasma facing component material at the University of Illinois," *Thin Solid Films*, Vol. 518, No. 22, September 2010, pp. 6663–6666.

[2]Feng-zhi, X., Geng-hua, C., Qian-sheng, Y., Mao-fu, Y., and Yin-an, L., "Superconducting film injected by ions from pulsed energetic dense plasma source," *J. Chinese Phys.*, Vol. 10, No. 11, November 2001, pp. 1049–53.

[3]Takeuchi, N., Yasuoka, K., and Shozo, I., "Surface modification of thin dielectric materials by compact theta-pinch plasma," Intl. Conference On Plasma Sci., IEEE, IEEE, Monterey, CA, Jun. 20-23 2005.

[4]Armstrong, W. T., Cochrane, J. C., Commisso, R. J., Lipson, J., and Tuszewski, M., "Theta-pinch ionization for field-reversed configuration formation," *Appl. Phys. Lett.*, Vol. 38, No. 9, May 1981, pp. 680–682.

[5]Taccetti, J. M., Intrator, T. P., Wurden, G. A., Zhang, S. Y., Aragonez, R., Assmus, P. N., Bass, C. M., Carey, C., deVries, S. A., Fienup, W. J., Furno, I., Hsu, S. C., Kozar, M. P., Langner, M. C., Liang, J., Maqueda, R. J., Martinez, R. A., Sanchez, P. G., Schoenberg, K. F., Scott, K. J., Siemon, R. E., Tejero, E. M., Trask, E. H., Tuszewski, M., Waganaar, W. J., Grabowski, C., Ruden, E. L., Degnan, J. H., Cavazos, T., Gale, D. G., and Sommars, W., "FRX-L: A field-reversed configuration plasma injector for magnetized target fusion," *Rev. Sci. Instrum.*, Vol. 74, No. 10, 2003, pp. 4314–4323.

[6]Grabowski, C., Degnan, J., Babineau, M., Camacho, F., Coffey, S., Coulter, G., Domonkos, M., Gale, D., Martinez, B., Parker, J., Ralph, D., Ruden, E., Sommars, W., Hsu, S., Intrator, T., Renneke, R., Sieck, P., Waganaar, B., and Wurden, G., "FRC compresion Heating Experiment (FRCHX) at AFRL," 16th Pulsed Power Conference, IEEE, Albuquerque, NM, 2007.

[7]Hallock, A. K., Choueiri, E. Y., and Polzin, K. A., "Current Sheet Formation in a Conical Theta Pinch Faraday Accelerator with Radio-frequency Assisted Discharge," 30th International Electric Propulsion Conference, ERPS, Florence, Italy, Sept. 17-20 2007.

[8]Niemela, C. S. and King, L. B., "Numerical optimization of an annular field reversed configuration translation experiment," 31st International Electric Propulsion Conference, ERPS, Univ. of Michigan, Ann Arbor, MI, 2009.

[9]White, J. S. and Scheeline, A., "Sampling and Excitation of Refractory Solids with a Theta Pinch Discharge Designed as an Atomic Emission Source," *Analytical Chem.*, Vol. 59, No. 2, January 1987, pp. 305–309.

[10]Pedrow, P. D. and Nasiruddin, A. M., "Experimental Study of CF4 Conical Theta Pinch Plasma Expanding into Vacuum," *Transactions on Plasma Science*, Vol. 17, No. 1, February 1989, pp. 17–23.

[11]Tuszewski, M., "Field Reversed Configurations," *Nuclear Fusion*, Vol. 28, No. 11, 1988, pp. 2033–2092.

[12]Steinhauer, L. C., "Review of field-reversed configurations," *Physics of Plasmas*, Vol. 18, No. 7, 2011, pp. 070501–1.

[13]Kirtley, D., Gallimore, A. D., Haas, J., and Reilly, M., "High Density Magnetized Toroid Formation and Translation

within XOCOT: An Annular Field Reversed Configuration Plasma Concept," 30th Intl. Electric Propulsion Conference, ERPS, ERPS, Florence, Italy, 2007.

[14]Hallock, A. K., Choueiri, E. Y., and Polzin, K. A., "Current Sheet Formation in a Conical Theta Pinch Faraday Accelerator with Radio-frequency Assisted Discharge," 44th Joint Propulsion Conference, AIAA, Hartford, CT, Jul. 21-23 2008.

[15]Little, E. M., Quinn, W. E., and Ribe, F. L., "Effects of Ionization and Magnetic Initial Conditions on a Magnetically Compressed Plasma (Scylla)," *Phys. Fluids*, Vol. 4, No. 6, June 1961, pp. 711–730.

[16]Commisso, R. J., Armstrong, W. T., Caldwell, J. C., Ekdahl, C. A., Lipson, J., Linford, R. K., Sherwood, E. G., Siemon, R. E., and Tuszewski, M., "The initial ionization stage of FRC formation," 1st Compact Toroid Symposium, Univ. of Calif., Los Alamos, NM, 1980.

[17]Milroy, R. D. and Brackbill, J. U., "Numerical Studies of a field-reversed theta-pinch plasma," *Physics of Fluids*, Vol. 25, No. 5, May 1982, pp. 775–783.

[18]Kirtley, D. E., *Study of the Synchronous Operation of an Annular Field Reversed Configuration Plasma Device*, Ph.D. thesis, Dept. of Aerospace Engineering, Univ. of Michigan, Ann Arbor, MI, 2008.

[19]Green, T. S. and Newton, A. A., "Diffusion of Antiparallel Bias Magnetic Field during the Initial Stages of a Theta-Pinch," *Phys. Fluids*, Vol. 9, No. 7, July 1966, pp. 1386–1388.

[20]Armstrong, W. T., Linford, R. K., Lipson, J., Platts, D. A., and Sherwood, E. G., "Field-Reversed Experiments (FRX) on Compact Toroids," *Physics of Fluids*, Vol. 24, No. 11, November 1981, pp. 2068–2089.

[21]Grabowski, C., Degnan, J. H., Amdahl, D. J., Delaney, R., Domonkos, M., Lehr, F. M., Magallanes, R., Robinson, P. R., Ruden, E. L., White, W., Wood, H., Gale, D., Kostora, M., McCullough, J., Sommars, W., Frese, M. H., Frese, S. D., Camacho, J. F., Coffey, S. K., Makhin, V., Intrator, T. P., Wurden, G. A., Sears, J., Turchi, P. J., Waganaar, W. J., Weber, T., Siemon, R. E., Fueling, S., Bauer, B. S., Lynn, A. G., and Roderick, N. F., "FRC Lifetime studies for the field reversed configuration heating experiment (FRCHX)," 53rd Plasma Physics Meeting, APS, Salt Lake City, UT, 2011.

[22]Wurden, G. A., Intrator, T. P., Zhang, S. Y., Furno, I. G., Hsu, S. C., Park, J. Y., Kirkpatrick, R., Renneke, R. M., Schoenberg, K. F., Taccetti, M. J., Tuszewski, M. G., Waganaar, W. J., Wang, Z., Siemon, R. E., Degnan, J. H., Gale, D. G., Grabowski, C., Ruden, E. L., Sommars, W., Frese, M. H., Coffey, S., Craddock, G., Frese, S. D., and Roderick, N. F., "FRC plasma studies on the FRX-L plasma injector for MTF," 20th Fusion Energy Conference, IAEA, Vilamoura, Portugal, November 2004.

[23]Meeks, W. C. and Rovey, J. L., "On the delayed gas breakdown in a ringing theta-pinch with bias magnetic field," *Physics of Plasmas*, Vol. 19, No. 5, 2012, pp. 052505.

[24]Verboncoeur, J. P., Langdon, A. B., and Gladd, N. T., "An object-oriented electromagnetic PIC code," *Comp. Phys. Comm.*, Vol. 87, 1995, pp. 199–211.

[25]Verboncoeur, J. P., "Particle simulation of plasmas: review and advances," *Plasma Phys. Control. Fusion*, Vol. 47, No. 5A, 2005, pp. A231–A260.

[26]Pahl, R. A. and Rovey, J. L., "Pre-Ionization Plasma in a FRC Test Article," No. AIAA-2012-0194 in 50th Aerospace Sciences Meeting, AIAA, Nashville, TN, 2012.

[27]Lobbia, R. B. and Gallimore, A. D., "High-speed dual Langmuir probe," *Review of Scientific Instruments*, Vol. 81, No. 7, 2010, pp. 073503.

[28]S. Humphries, J., Anderson, R. J. M., Freeman, J. R., and Greenly, J., "Pulsed plasma guns for intense ion beam injectors," *Review of Scientific Instruments*, Vol. 52, No. 2, 1981, pp. 162–171.